Variability of Child Rib Bone Hounsfield Units using in vivo Computed Tomography

Baptiste Sandoz, Zaki Sidelkeir, Alina Badina, François Bermond, David Mitton, Wafa Skalli

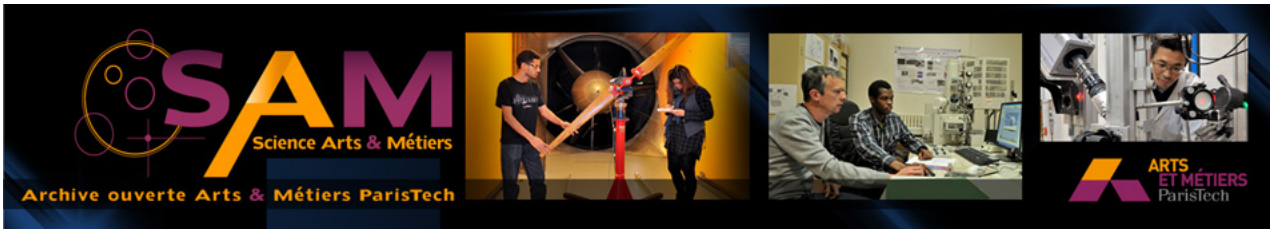

Variability of Child Rib Bone Hounsfield Units using *in vivo* Computed Tomography

Baptiste Sandoz, Zaki Sidelkeir, Alina Badina, François Bermond, David Mitton, Wafa Skalli

Abstract The variability assessment of the rib bone mechanical properties during the growth process is still missing. These properties could not be obtained *in vivo* on children. Relationships have been obtained between Hounsfield Units from computed tomography (CT) and mechanical properties (e.g. for the cortical bone on adults). As a first step for investigation of the mechanical properties of child ribs, the aim of this study was to determine the Hounsfield Units variation of child ribs from CT-scan data, by rib level, along the rib and within the rib sections. Twenty-seven right ribs of levels 4, 6 and 9 were processed from 11 thoracic CT scans of children without bone lesions aged between 1 and 10 years. A first set of 10 equidistributed cross-sections normal to the rib midline were extracted. Sixteen equally distributed elements defined 4 areas into the cortical band: internal, external, caudal and cranial. Within the rib sections, Hounsfield Units were found significantly higher in internal and external areas than in caudal and cranial. In a further step using calibrated CT scans, it would be possible to derive the mechanical properties of *in vivo* child ribs using bone density correlation with Hounsfield Units.

Keywords child, CT-scans, Hounsfield Units, ribs

I. INTRODUCTION

Thoracic trauma is one of the major causes of fatalities and injuries in car crashes. The thorax is the second most frequently injured region after the head [1]. In order to improve public safety a better knowledge of the rib cage biomechanics is needed [2-4]. Models developed using biomechanical knowledge have been mainly focused on average individuals (e.g. 50th percentile male) [5-6]. However, the entire population from children to the elderly should be better protected. Thus specific thorax models have been developed for children [7-8] and for adults taking into account the aging effect [9-10].

To build a finite element model of the rib cage, data for the geometry and the mechanical properties of the biological tissues are required. The geometry of the rib cage can be obtained from medical imaging (e.g. using biplanar X-rays [11-14]).

The rib mechanical properties can be assessed from mechanical experiments on cadaver specimens. In most of the cases, elderly subjects have been considered. Assessing the mechanical properties of the rib non-invasively in children *in vivo* is still a scientific bottleneck. Elasticity-density (obtained from quantitative computed tomography) relationships have been found either on vertebral cancellous bone [15] or on femoral cortical bone [16]), but no similar relationships have been proposed for the ribs. Assuming that, in a preliminary approach, the relationship assessed on femoral cortical bone could be extended to the rib cortical bone, the measurement of the rib density would allow their mechanical properties to be derived. Today quantitative computed tomography is the only clinical modality that could allow detailed rib density measurement. A calibration step is required to assess bone density from the Hounsfield Units (HU). Despite the fact that clinical exams performed under medical prescriptions are uncalibrated from a bone density point of view, they provide access to the grey levels (HU) thus allowing a first step towards mechanical properties assessment *in vivo*.

The aims of this study are 1) to propose a methodology to extract Hounsfield Units from specific locations of the ribs and 2) to assess the variability of the Hounsfield Units in a cross-section of a rib and along a rib from the vertebrae to the sternum.

B. Sandoz is Assistant Professor, Z. Sidelkeir is student on the MSc in Bioemechanics and W. Skalli is Professor at Arts et Metiers ParisTech, LBM, 151 bd de l'hopital, 75013 Paris, France (baptiste.sandoz@ensam.eu +33144246364). A. Badina is Medical Doctor at Université Paris Descartes, Faculté de Médecine, Hôpital Necker, Service d'orthopédie pédiatrique, 149 rue de Sèvre, 75015, Paris, France. F. Bermond is researcher and D. Mitton is Research Director at Université de Lyon, F-69622, Lyon; IFSTTAR, UMR_T9406, LBMC, Bron; Université Lyon 1, Villeurbanne, France.

II. METHODS

Population

In accordance with the Internal Review Board of Paris Descartes University, eleven thoracic helical CT scans of children aged from 1 to 10 years (5 girls, 6 boys) were taken from a larger anonymized database (Necker Hospital Paris, France) [17]. The CT scans had previously been performed on prescriptions which were: severe asthma, acute respiratory distress syndrome, investigation of intrathoracic lymph nodes, inhaled foreign body, trauma with no bone lesion, staging of primary extra-thoracic malignancies. CT scans in children with syndromes or heart congenital lesions were excluded. CT scans showing thoracic abnormalities or recent surgery were not included. The 3D reconstructions of the external contours of the ribs had already been performed and validated [17]. Twenty-seven right ribs of levels 4 (n=8), 6 (n=10) and 9 (n=9) were studied, as shown in Table 1. All the images were contiguous, obtained with the same scanner (GE Medical System, LightSpeed VCT) and same resolution (512*512 pixels).

Table 1: Age, gender and right ribs levels studied; CT images slice thickness and pixel size.

Scan n°	Age (year)	gender	Right rib level	Slice Thickness (mm)	Pixel size (mm)
1	1	F	4 6 9	0.625	0,316
2	1	F	4 6	1.25	0,391
3	3	F	4 6 9	1.25	0,395
4	3	M	4 6 9	1.25	0,391
5	3	M	9	1.25	0,410
6	6	F	6 9	1.25	0,420
7	6	F	4 6	1.25	0,506
8	6	M	4 6 9	1.25	0,412
9	10	M	4 6 9	1.25	0,547
10	10	M	6 9	1.25	0,506
11	10	M	4 6 9	1.25	0,486

Slice extraction and orientation

These standard CT images were made in the transverse plane of the patients. In order to extract 100 equidistant slices along the ribs, perpendicular to their midlines, the images have been re-sliced using a combination of the 3D reconstructions of the external contours of the ribs already performed and validated [17]. Due to this new 3D orientation of the slices, a trilinear approximation of the closest pixels was used in order to define the pixel Hounsfield Units (HU) of these new images, with respect to the initial HU of the CT scan. The local frame (position and orientation) was then calculated for each of these slices, with respect to the CT-scan frame (Figures 1a and 1b).

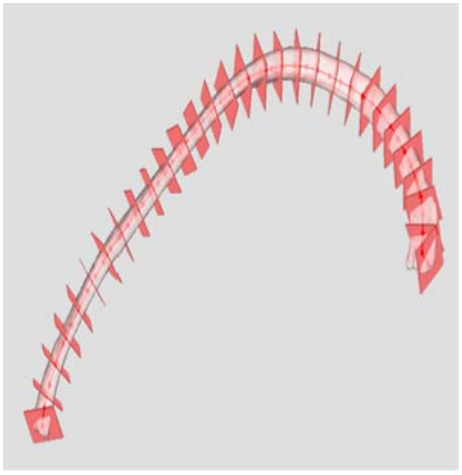

Figure 1a: Some of the 100 equidistant slices, perpendicular to the rib midline

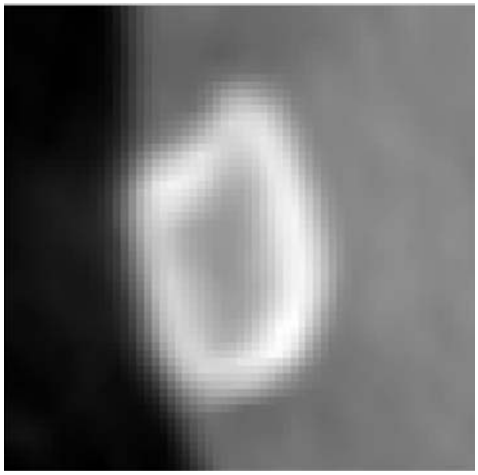

Figure 1b: One output slice perpendicular to the rib midline

Hounsfield Units measurement into the cortical bone

As a first approach, the cortical bone was studied using Matlab© (Mathworks, v2011b). Contours were defined on each slice, using an automatic gradient detection with manual control of the gradient threshold (Figures 2). The external contour was automatically detected and approximated by 50 points. The pixel HU profile was extracted from each point of the external contour to its center. The internal contour was defined when the pixel HU fit with the chosen threshold.

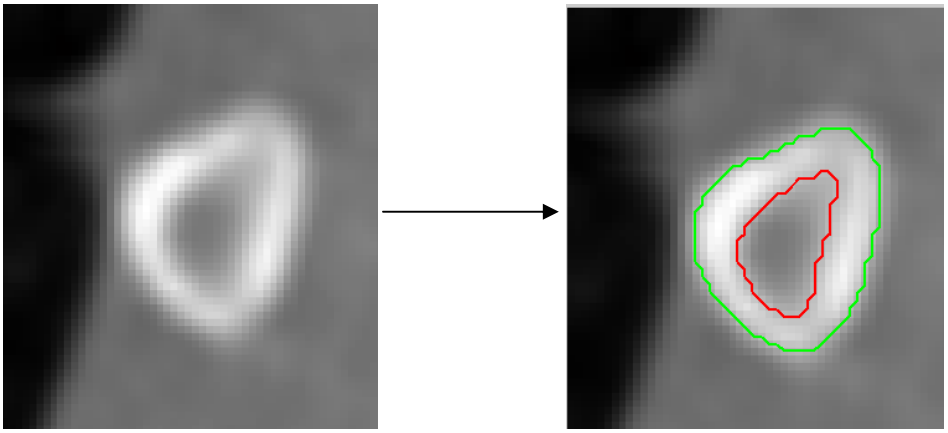

Figure 2: Detection of external (green) and internal (red) contours based on gradient detection

This manual control was made only by one operator and no variability study was performed. However, in order to avoid the edge effects of this detection and to ensure location at the cortical bone, the Region Of Interest (ROI) was defined as an inner cortical band based on a mid-contour: 17 equally distributed points were defined on the internal and external contours and the mid-contour was defined by the mid-points (Figure 3a, blue line). Then, the inner cortical band defined the ROI as the 50% inner part around the mid-contour (Figure 3b, black lines).

a. 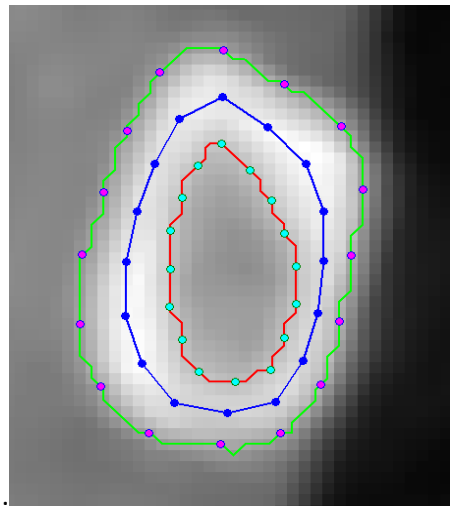 b. 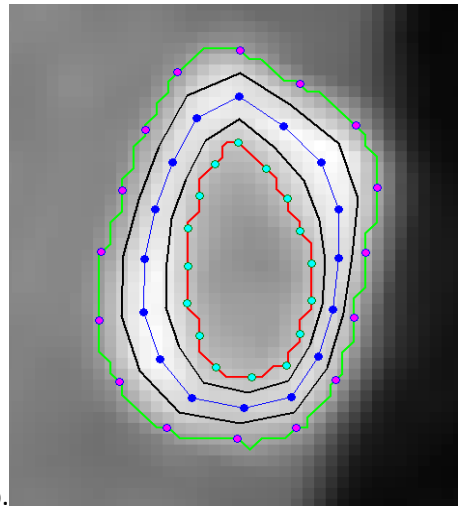

Figure 3: External contour (green), internal contour (red), medium contour (blue) and ROI (cortical band, black).

Finally, 16 elements equally distributed were built and the HU of the pixels entirely within these elements were studied (Figure 4). Four areas were then defined: cranial, caudal, internal and external. For each studied rib, 10 equally spaced slices were analyzed from 5% to 95% of its length, from the vertebral to the sternal junctions.

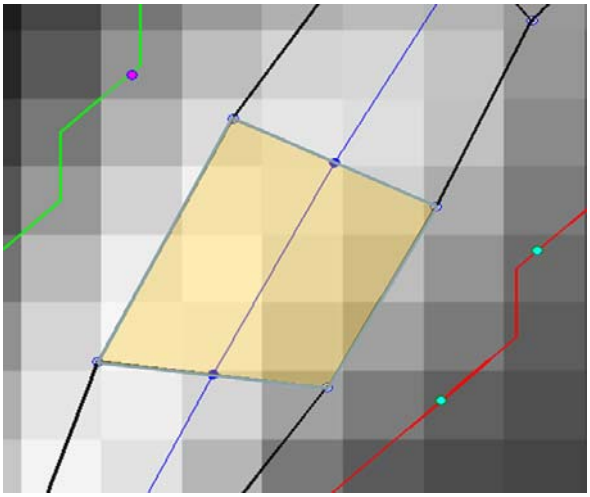

Figure 4: Zoom of figure 3. One element in yellow superimposed to the pixels (grey levels).

Statistical analyses (Student's paired t-test) were performed on the HU of the previous studied pixels, in order to assess the statistical significance of differences regarding their location (caudal-cranial and internal-external) and rib levels (4^{th}, 6^{th} and 9^{th}).

III. RESULTS

Hounsfield Units distribution by area

HU is significantly higher in external and internal than in caudal and cranial areas ($p<10^{-14}$) for all ribs and all subjects. Figure 5 shows an example of the HU variation in one slice, by area.

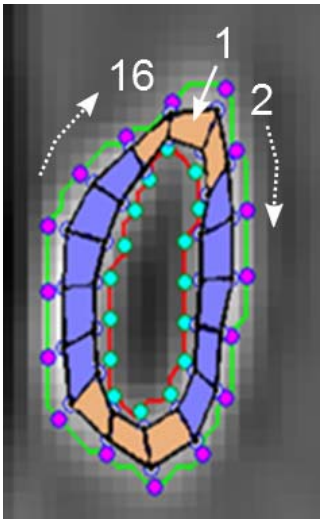

Figure 5a: Subject 9, elements within one rib section

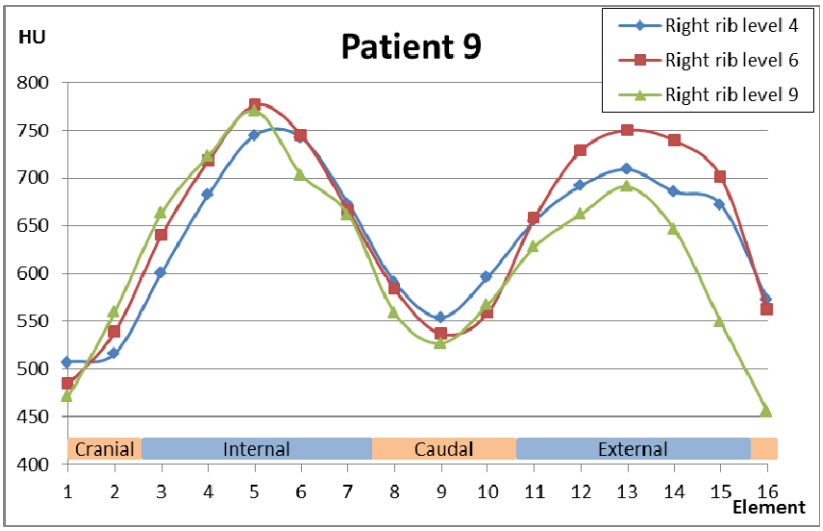

Figure 5b: Subject 9, mean Hounsfield Units (HU) within the rib sections

Hounsfield Units variation along the ribs

Considering the mean HU in each slice, the HU increase from the vertebral junction to the first 45% of the rib length and decrease afterward, until the sternal junction extremity (Figure 6). These variations are observed for all levels of all subjects (see appendix).

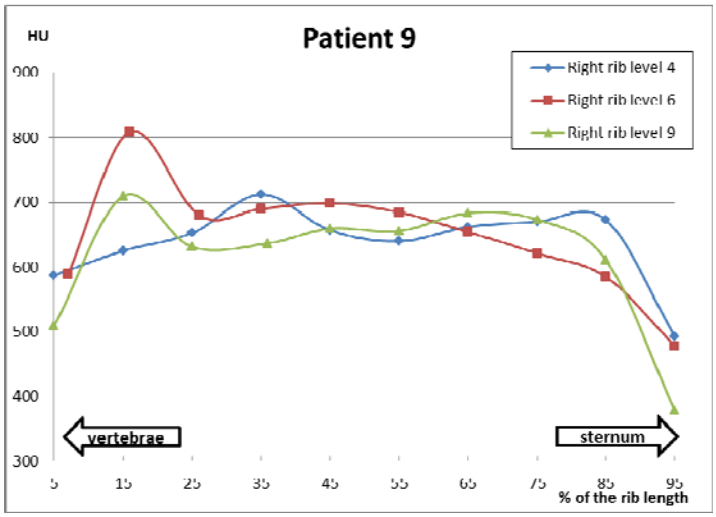

Figure 6: Subject 9 – mean Hounsfield Units (HU) by rib level from vertebral to sternal joint

Hounsfield Units variation by rib level

In the studied population, the mean HU of the 6th rib level is higher than both the 4th (p=0.068) and the 9th level (p=0.023). This result is summarized in Table 2.

Table 2: Mean Hounsfield Units (HU) by rib level

Subject	Rib level		
	4	6	9
1	973	982	977
2	865	894	-
3	904	953	911
4	905	905	879
5	-	-	553
6	-	1150	1102
7	717	761	-
8	1021	1055	1042
9	637	649	614
10	-	588	586
11	648	645	652

IV. DISCUSSION

This study proposed a methodology to extract Hounsfield Units of a cortical band of child ribs from *in vivo* CT scans and to study the variability of these HU in a cross section as well as along the rib from the vertebrae to the sternum. Thus, in order to avoid edge uncertainties within a cross section, a cortical band made of 16 elements was defined as the 50% inner part between the internal and external contour. Even if this first approach considered only the pixels entirely within the elements, a significant variation of the HU was observed. The internal and external areas have higher HU than the caudal and cranial.

Moreover, the HU varied along the rib length. From the vertebral junction, the HU increased for the first half of the rib and then decreased until the sternal junction. The HU is higher in the lateral region than in the anterior and posterior regions. This result could be analyzed in light of the results obtained by Stitzel et al. [3] regarding the average stiffness and average ultimate stress for the cortical bone specimens located in the lateral (11.9 GPa modulus, 153.5 MPa ultimate stress) portion of the ribs versus the anterior (7.51 GPa, 116.7 MPa) and posterior (10.7 GPa, 127.7 MPa) rib locations. Finally, the mean HU of the entire rib is slightly higher for the 6^{th} rib level than the 4^{th} (2.6% in average) and the 9^{th} (2.3% in average).

Because CT scans were not calibrated, it is not possible to draw any conclusion regarding the age effect. However, the calibration procedure provides the description of a linear relationship between HU and actual bone density, and therefore the present methodology gave some indications within the subjects that have to be further refined using calibrated data. The present methodology can then be applied to any standard CT-scan image and will be the first step to link the HU, the bone density and the mechanical behavior of human ribs.

V. CONCLUSIONS

The present study gives for the first time the *in vivo* estimation of the child Hounsfield Units variation within rib cross sections, along the rib length and by rib level. Future work is planned to link the Hounsfield Units to bone density using calibrated CT-scans, then to mechanical properties performed *ex vivo* on adult specimens. It will then be possible to calculate the mechanical properties of *in vivo* child ribs and other bones.

VI. ACKNOWLEDGEMENT

Authors wish to thank B. Aubert for its invaluable technical support.

VII. REFERENCES

[1] Weninger P and Hertz H, Factors influencing the injury pattern and injury severity after high speed motor vehicle accident--a retrospective study, *Resuscitation*, 75(1):35-41, 2007.

[2] Kemper AR, McNally C, et al., Material properties of human rib cortical bone from dynamic tension coupon testing. *Stapp Car Crash J*, 49:199-230, 2005.

[3] Stitzel JD, Cormier JM, et al., Defining regional variation in the material properties of human rib cortical bone and its effect on fracture prediction, *Stapp Car Crash J*, 47:243-65, 2003.

[4] Vezin P and Berthet F, Structural characterization of human rib cage behavior under dynamic loading. *Stapp Car Crash J*, 53:93-125, 2009.

[5] Ruan J, El-Jawahri R, Chai L, Barbat S and Prasad P, Prediction and analysis of human thoracic impact responses and injuries in cadaver impacts using a full human body finite element model, *Stapp Car Crash J*, 47:299-321, 2003.

[6] Song E, Trosseille X, and Baudrit P, Evaluation of thoracic deflection as an injury criterion for side impact using a finite elements thorax model, *Stapp Car Crash J*, 53:155-91, 2009.

[7] Jiang B, Cao L, et al., Development of a 10-year-old paediatric thorax finite element model validated against cardiopulmonary resuscitation data, *Comput Methods Biomech Biomed Engin*, 10.1080/10255842.2012.739164, 2012, *in press*.

[8] Mizuno K, Iwata K, Deguchi T, Ikami T and Kubota M, Development of a three-year-old child FE mode,. *Traffic Inj Prev*, 6(4):361-71, 2005.

[9] El-Jawahri RE, Laituri TR, Ruan JS, Rouhana SW and Barbat SD, Development and validation of age-dependent FE human models of a mid-sized male thorax, *Stapp Car Crash J*, 54:407-30, 2010.

[10] Forman JL, Kent RW, et al., Predicting rib fracture risk with whole-body finite element models: development and preliminary evaluation of a probabilistic analytical framework, *Ann Adv Automot Med*, 56:109-24, 2012.

[11] Benameur S, Mignotte M, Destrempes F, and De Guise JA, Three-dimensional biplanar reconstruction of scoliotic rib cage using the estimation of a mixture of probabilistic prior model, *IEEE Trans Biomed Eng*, 52(10): 1713-28, 2005.

[12] Dansereau J and Stokes IA, Measurements of the three-dimensional shape of the rib cage, *J Biomech*, 21(11): 893-

901, 1988.
[13] Jolivet E, Sandoz B, Laporte S, Mitton D and Skalli W, Fast 3D reconstruction of the rib cage from biplanar radiograph, *Med Biol Eng Comput*, 48(8):821-8, 2010.
[14] Mitton D, Zhao K, et al., 3D reconstruction of the ribs from lateral and frontal X-rays in comparison to 3D CT-scan reconstruction, *J Biomech*, 41(3):706-10, 2008.
[15] Kopperdahl DL, Morgan EF and Keaveny TM, Quantitative computed tomography estimates of the mechanical properties of human vertebral trabecular bone, *J Orthop Res*, 20*(*4):801-5, 2002.
[16] Duchemin L, Bousson V, et al., Prediction of mechanical properties of cortical bone by quantitative computed tomography, *Med Eng Phys*, 30(3):321-8, 2008.
[17] Sandoz B, Badina A, et al., Quantitative geometric analysis of rib, costal cartilage and sternum from childhood to teenagehood, *Med Biol Eng Comput*, 10.1007/s11517-013-1070-5, 2013.

APPENDIX

Mean HU within the rib sections	Mean HU by rib level from vertebral to sternal joint

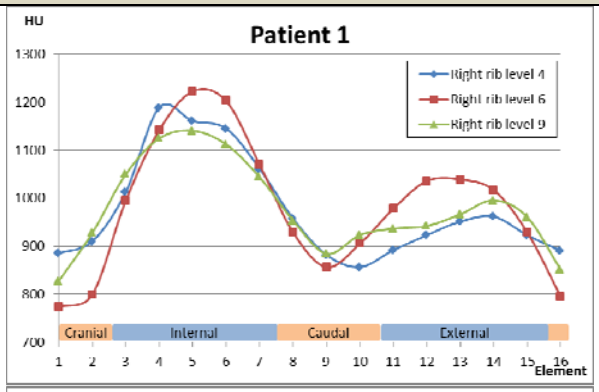

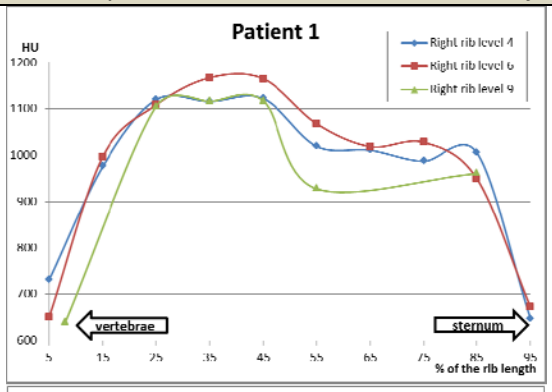

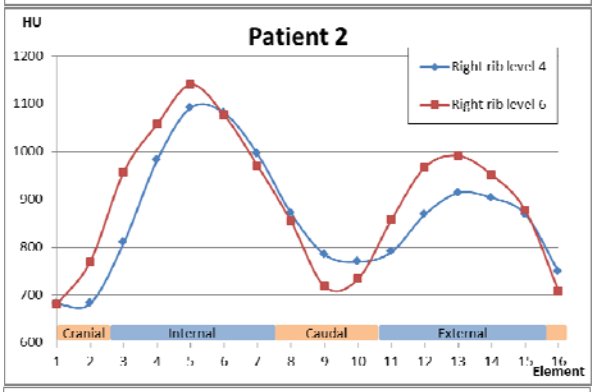

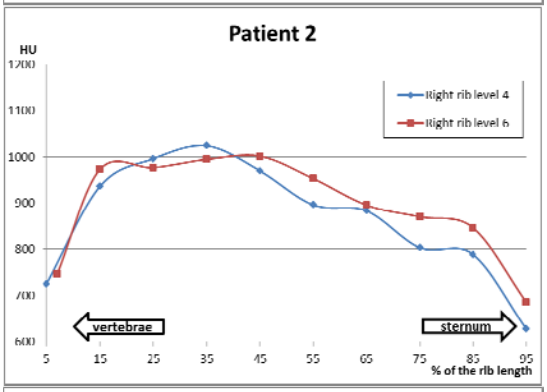

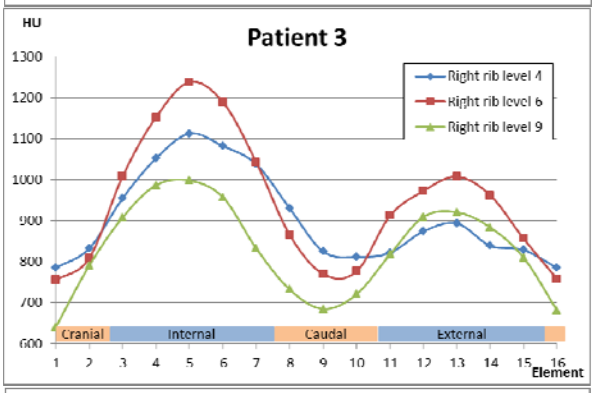

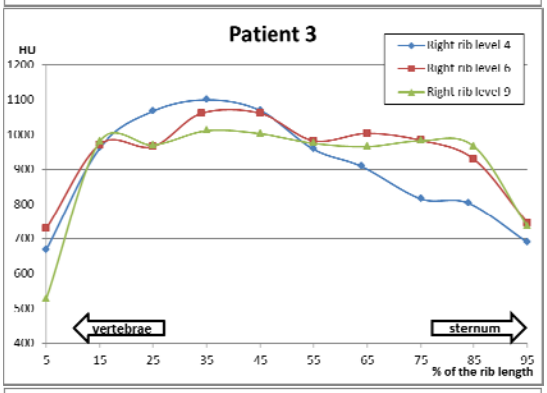

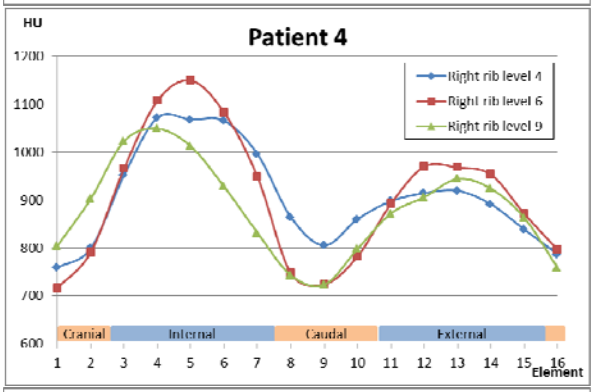

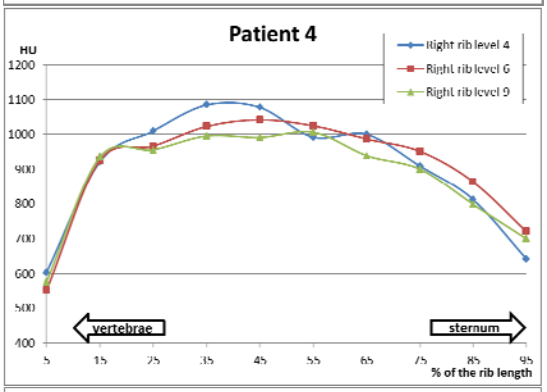

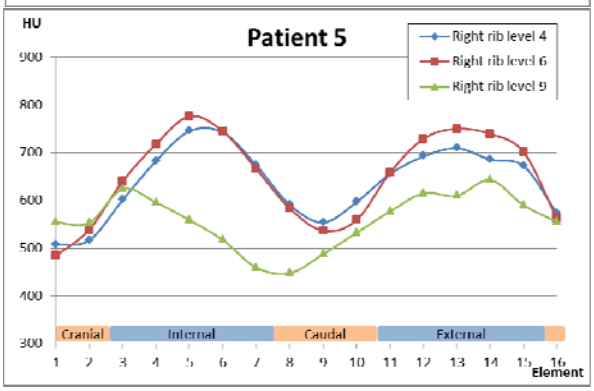

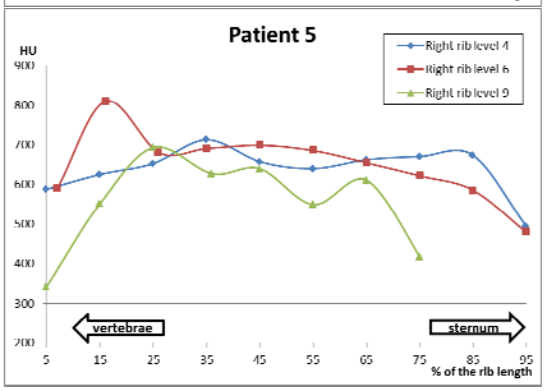

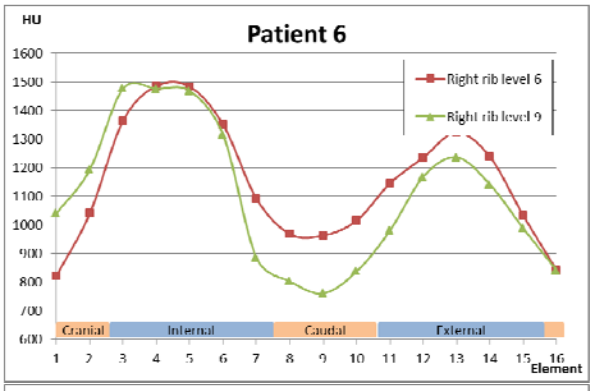
Patient 6
HU
Right rib level 6
Right rib level 9
Cranial
Internal
Caudal
External
Element

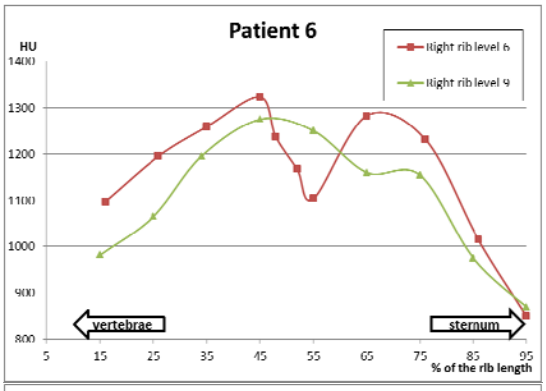
Patient 6
HU
Right rib level 6
Right rib level 9
vertebrae
sternum
% of the rib length

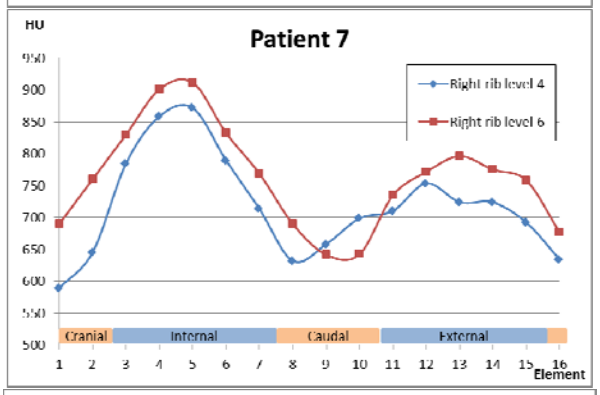
Patient 7
HU
Right rib level 4
Right rib level 6
Cranial
Internal
Caudal
External
Element

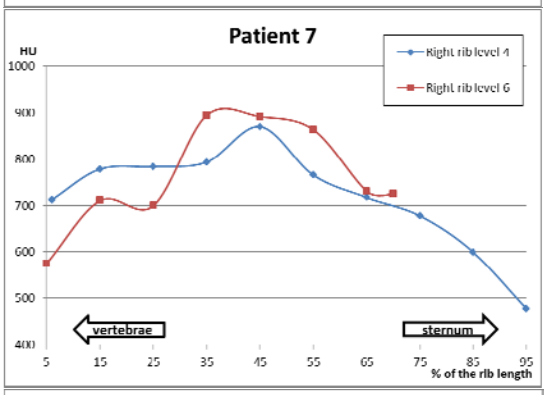
Patient 7
HU
Right rib level 4
Right rib level 6
vertebrae
sternum
% of the rib length

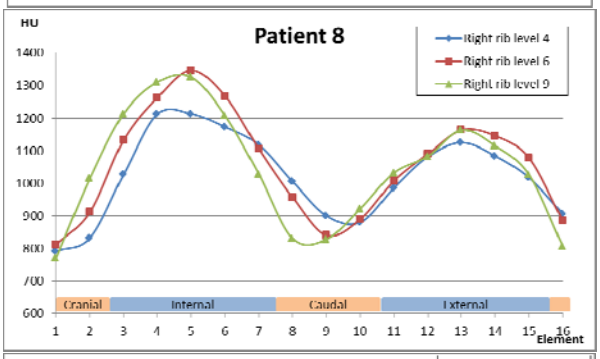
Patient 8
HU
Right rib level 4
Right rib level 6
Right rib level 9
Cranial
Internal
Caudal
External
Element

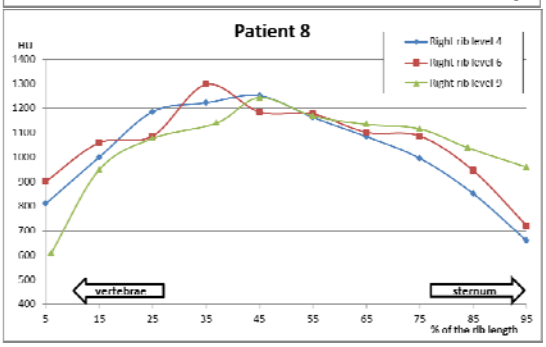
Patient 8
HU
vertebrae
sternum
% of the rib length

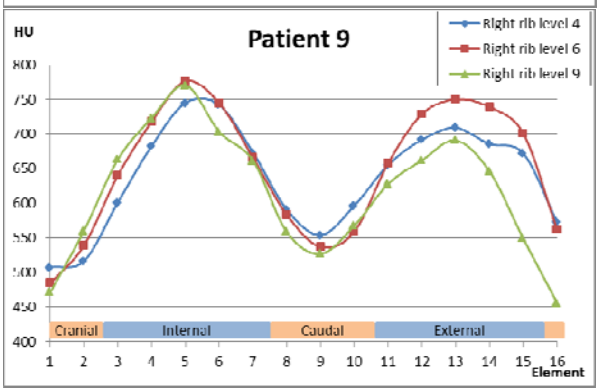
Patient 9
HU
Right rib level 4
Right rib level 6
Right rib level 9
Cranial
Internal
Caudal
External
Element

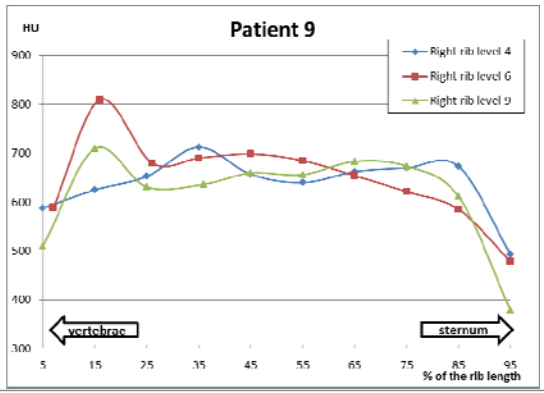
Patient 9
HU
Right rib level 4
Right rib level 6
Right rib level 9
vertebrae
sternum
% of the rib length

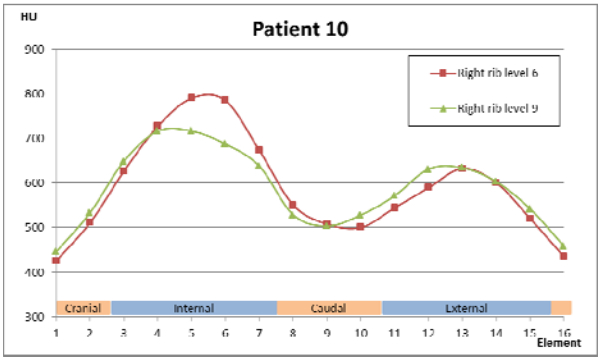
Patient 10
HU
Right rib level 6
Right rib level 9
Cranial
Internal
Caudal
External
Element

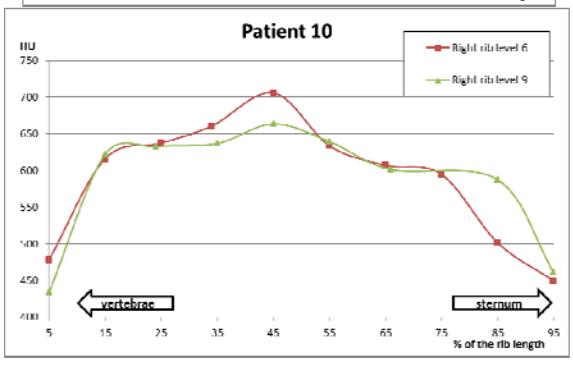
Patient 10
HU
Right rib level 6
Right rib level 9
vertebrae
sternum
% of the rib length

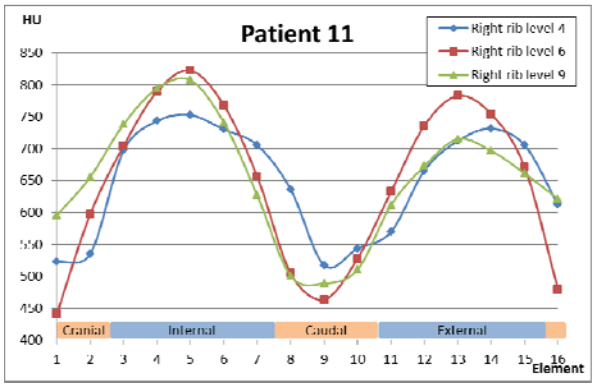
Patient 11
HU
Right rib level 4
Right rib level 6
Right rib level 9
Cranial
Internal
Caudal
External
Element

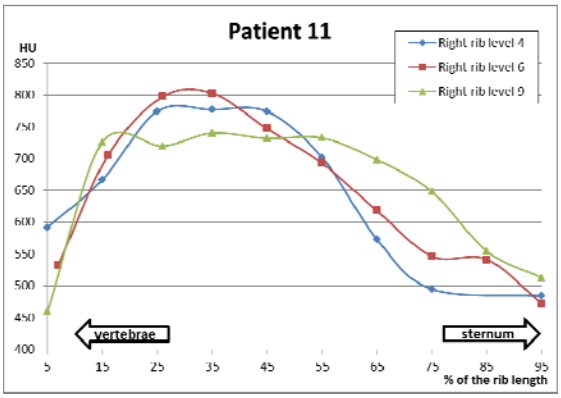
Patient 11
HU
Right rib level 4
Right rib level 6
Right rib level 9
vertebrae
sternum
% of the rib length